Contents lists available at ScienceDirect

Water Research

journal homepage: www.elsevier.com/locate/watres





The sanitary sewer unit hydrograph model: A comprehensive tool for wastewater flow modeling and inflow-infiltration simulations

Gabriel Perez a,*, Jesus D. Gomez-Velez b,a,c,**, Stanley B. Grant c

- ^a Department of Civil & Environmental Engineering, Vanderbilt University, Nashville, TN, 37205, United States
- b Environmental Sciences Division & Climate Change Science Institute, Oak Ridge National Laboratory, Oak Ridge, TN, 37830, United States
- ^c Occoquan Watershed Monitoring Laboratory, Department of Civil & Environmental Engineering, Virginia Tech, Manassas VA, 9408, United States

ARTICLE INFO

Dataset link: https://github.com/gomezvelezlab/SanitarySewer-WFIUH

Keywords:
Weighted width function
Unit hydrograph
Sewer network
Base wastewater flow
Groundwater infiltration
Runoff derived infiltration and inflow

ABSTRACT

Sanitary sewer systems are critical urban water infrastructure that protect both human and environmental health. Their design, operation, and monitoring require novel modeling techniques that capture dominant processes while allowing for computationally efficient simulations. Open water flow in sewers and rivers are intrinsically similar processes. With this in mind, we formulated a new parsimonious model inspired by the Width Function Instantaneous Unit Hydrograph (WFIUH) approach, widely used to predict rainfall-runoff relationships in watersheds, to a sanitary sewer system consisting of nearly 10,000 sewer conduits and 120,000 residential and commercial sewage connections in Northern Virginia, U.S.A. Model predictions for the three primary components of sanitary flow, including Base Wastewater Flow (BWF), Groundwater Infiltration (GWI), and Runoff Derived Infiltration and Inflow (RDII), compare favorably with the more computationally demanding industry-standard Storm Water Management Model (SWMM). This novel application of the WFIUH modeling framework should support a number of critical water quality endpoints, including (i) sewer hydrograph separation through the quantification of BWF, GWI, and RDII outflows, (ii) evaluation of the impact of new urban developments on sewage flow dynamics, (iii) monitoring and mitigation of sanitary sewer overflows, and (iv) design and interpretation of wastewater surveillance studies.

1. Introduction

Sanitary sewers convey wastewater from residential and non-residential users to treatment facilities prior to re-use for non-potable or potable purposes or disposal to inland or coastal waters. In addition to these so-called base wastewater flows (BWF), sanitary sewage collection systems also accumulate extraneous flows in the form of groundwater infiltration (GWI) and rainfall-derived inflow and infiltration (RDII). These extraneous flows vastly increase the energy and carbon footprint costs of wastewater treatment (Hey, Gerly and Jönsson and Mattsson, 2016; Lai, 2008; Grant et al., 2012), the frequency of sewage overflow events (Sojobi and Zayed, 2022), and complicate the design and interpretation of epidemiological wastewater surveillance programs (Gonzalez et al., 2020). The contribution of GWI and RDII to sewer flows varies by site depending on the local hydrogeology and

climate (Pangle et al., 2022; Nasrin et al., 2017), as well structural deterioration of the sewage collection network (e.g., leaking pipes) and illicit connections of storm drains into sanitary sewers (Lai, 2008; Selvakumar et al., 2004; Karpf and Krebs, 2011). Simple and scalable methods for estimating the BWF, GWI, and RDII components of sewage flows under various population growth, climate change, and management scenarios are urgently needed.

Back-of-the-envelope estimates of BWF can be calculated from metered water consumption data by assuming that a fixed fraction of the consumed water, commonly 90% (Butler et al., 2018), is returned to the sanitary sewer system. In reality, the return fraction varies depending on a number of site-specific factors, including the mix of residential and commercial connections in a particular sewage collection network, average household size, and the frequency of indoor and outdoor water

E-mail addresses: perezmesagj@ornl.gov (G. Perez), gomezvelezjd@ornl.gov (J.D. Gomez-Velez).

https://doi.org/10.1016/j.watres.2023.120997

Received 26 July 2023; Received in revised form 19 November 2023; Accepted 7 December 2023 Available online 8 December 2023

0043-1354/© 2023 The Authors. Published by Elsevier Ltd. This is an open access article under the CC BY-NC license (http://creativecommons.org/licenses/by-nc/4.0/).

Notice: This manuscript has been co-authored by staff from UT-Battelle, LLC, under contract DE-AC05-00OR22725 with the US Department of Energy (DOE). The US government retains and the publisher, by accepting the article for publication, acknowledges that the US government retains a nonexclusive, paid-up, irrevocable, worldwide license to publish or reproduce the published form of this manuscript, or allow others to do so, for US government purposes. DOE will provide public access to these results of federally sponsored research in accordance with the DOE Public Access Plan (http://energy.gov/downloads/doe-public-access-plan).

^{*} Correspondence to: Environmental Sciences Division, Oak Ridge National Laboratory, Oak Ridge, TN, 37830, United States.

^{**} Corresponding author.

| Abbreviations | and | eymbol | |
|---------------|-----|--------|---|
| Abbreviations | anu | symbol | S |

| SS-WFIUH | Sanitary | Sewer | Width | Function | Instanta- |
|----------|----------|-------|-------|----------|-----------|
|----------|----------|-------|-------|----------|-----------|

neous Unit Hydrograph

BWF Base Wastewater Flow GWI Groundwater Infiltration

RDII Runoff Derived Infiltration and Inflow SWMM Storm Water Management Model RTK Unit hydrograph method RTK I/I Inflow and Infiltration

I/I Inflow and Infiltration
TAZ Transportation Analysis Zones

nSewer network nodeOSewershed outlet Q_O Total outflow at O $Q_{BWF,O}$ Outflow of BWF at O $Q_{GWI,O}$ Outflow of GWI at O $Q_{RDII,O}$ Outflow of RDII at O

 $egin{array}{ll} Q_{RDII_{fast},O} & ext{Fast response component of } Q_{RDII,O}(t) \ Q_{RDII_{slow},O} & ext{Slow response component of } Q_{RDII,O}(t) \ k & ext{Type of flow: BWF, GWI, or RDII} \ \end{array}$

 $g_{O,k}$ Transfer function for the kth type of flow

for the sewershed at O

 $Q_{I,k}$ Time-varying Input for the kth type of flow $W_{O,k}$ Network's width function at O for the kth

type of flow

 u_k Celerity of a flood wave for type of flow k D_k Coefficient of hydrodynamic dispersion for

type of flow k

 $L_{O,k,max}$ Longest flow path through the network at

o

 J_{BWF} Per person wastewater input flow

 N_O Number of people contributing sewage to

the network upstream at O

DF(t) Demand factor

 $ar{q}_{BWF}$ Average per capita daily BWF $Q_{O.{
m dry}}$ Dry weather sewage outflow at O

 $t_{O,h}$ Time shift

 $t_{O, \mathrm{peak}}$ Time of day when the measured outflow

peaks

 $t_{DF, \mathrm{peak}}$ Time of day when the demand factor peaks $Q_{O, \mathrm{dry, \; min}}$ Minimum dry weather flow measured at O Average dry weather flow measured at O

 A_1 Calibration constant A_O Total area that drains to O

 L_O Total conduit length that drains to O J_{GWLA} Input groundwater flux per unit draining

area

 $J_{GWI,L}$ Input groundwater flux per unit length of

conduit

 $\begin{array}{ll} J_{RDII_{fast}} & & \text{Input flow of RDII}_{fast} \\ J_{RDII_{slaw}} & & \text{Input flow of RDII}_{slow} \end{array}$

 R_{fast} Fraction of precipitation that becomes RDII

for the fast response

 R_{slow} Fraction of precipitation that becomes RDII

for the slow response

P Precipitation

 d_0 Diameter of the circular cross-section

 v_I Initial flow velocity

| B_I | Initial water surface width |
|-------------------------|---|
| $	heta_I$ | Initial slope of the water surface |
| R_I | Initial hydraulic radius |
| S_0 | Conduit slope |
| F | Froude number |
| $Q_{O,\mathrm{RDII}}^*$ | Observed RDII |
| ΔQ_{BWF} | Expected variation of $Q_{O,dry, ave}$ |
| DF_{min} | Minimum demand factor |
| $t_{DF,peak}$ | Time of the morning peak for water consumption |
| \bar{t}_h | Average hydraulic response time for the sewershed |

use, which is related to local climate (Jacobs and Haarhoff, 2004). Obtaining realistic estimates of GWI and RDII, collectively known as inflow and infiltration (I/I), is even more challenging and can be a major source of uncertainty in evaluating the costs and benefits of sewer replacement programs and long-range planning for sewage treatment facilities, particularly in the face of climate change (Zhang et al., 2018a,b; Beheshti et al., 2015).

Unit hydrograph theory is a well-known framework for modeling rainfall-runoff events in watershed systems. The similarities between natural river systems and sewer systems have inspired applications of the theory for predicting I/I in urban stormwater and sewage collection systems. For example, the RTK method, which is based on triangular unit hydrographs, is one of the most popular methods used by practitioners to estimate I/I and has been incorporated into the EPA SWMM and SSOAP software package (Lai, 2008; Vallabhaneni and Burgess, 2007). Among the multiple formulations derived from the seminal paper describing the unit hydrograph (Sherman, 1932), the width function instantaneous unit hydrograph (WFIUH) is a robust and flexible formulation that captures key hydrodynamic processes controlling runoff routing in watershed systems (Rigon et al., 2016). The WFIUH modeling framework has been used to represent diverse physical mechanisms affecting streamflow responses, including drainage density (Mutzner et al., 2016; Di Lazzaro et al., 2015), meltwaters (Yang et al., 2018), storm trajectory (Volpi et al., 2013; Perez et al., 2023), and even the effect of reservoirs and lakes in the runoff routing for large basin scales (Piccolroaz et al., 2016).

In this paper, we develop and test a novel application of WFIUH theory for modeling sanitary sewer (SS) flows, a framework we refer to as SS-WFIUH. Specifically, we: (i) formulate the fundamental equations required to predict BWF, GWI, and RDII fluxes in a sanitary sewer system; (ii) calibrate the SS-WFIUH model using hourly measurements of sanitary flow from a moderately sized (≈100,000 connections) and mostly residential sanitary sewage collection system in Northern Virginia, U.S.A; and (iii) validate the performance of the SS-WFIUH framework by comparison to hourly sewer flow measurements and predictions from the more computationally demanding industry standard Storm Water Management Model (SWMM) modeling system (Vallabhaneni and Burgess, 2007). Our modeling framework is notable in its conceptual simplicity, computational efficiency, and scalability to sewer networks of arbitrary complexity and size.

2. Model formulation

Sanitary sewer networks can be conceptualized as open channel systems composed of sewer conduits (links) connected through manholes (nodes) in a tree-like structure draining to a discharge point, commonly a pump station or wastewater treatment plant (Fig. 1). The network structure typically includes: (i) the main sewer line, which is the primary conduit through which sewage from all connections flows

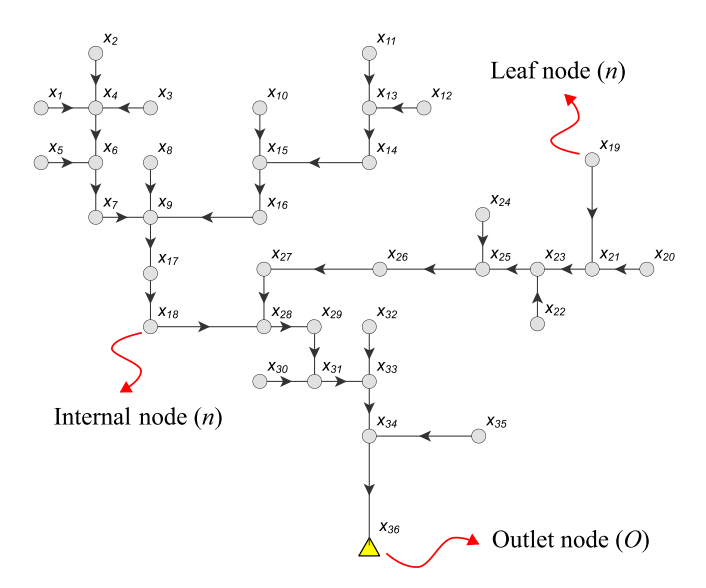


Fig. 1. Sketch of a sewershed layout with 36 nodes (*n*) highlighting the location of leaf and internal nodes and the sewershed outlet, *O*. Arrows depict the flow direction in sewer pipes.

to the discharge point; and (ii) local drain lines that convey the sewage from individual connections (e.g., residential units or commercial and industrial facilities) to the main sewer line. Due to a lack of data at the scale of individual connections, the analysis of sewer network hydraulics is typically focused on the main sewer line, while local drain lines are represented as a spatially variable collection of sewage inputs. Ignoring local drain lines is not expected to significantly impact our modeling results because these lines typically involve short travel times from the input to the main sewer line, and thus have a minor impact on the system's width function.

2.1. Mathematical framework

The total outflow from the sewer network, $Q_O(t)$ [L³T⁻¹], is the sum of BWF, $Q_{BWF,O}(t)$ [L³T⁻¹], GWI, $Q_{GWI,O}(t)$ [L³T⁻¹], and RDII, $Q_{\text{RDII},O}(t)$ [L³T⁻¹] components. Typically, infiltration processes extend beyond the end of the rainfall event (US Environmental Protection Agency, 2014). Consequently, it is convenient to separate RDII into fast ($Q_{RDII_{fast},O}(t)$) and slow ($Q_{RDII_{slow},O}(t)$) responses. Then, under the SS-WFIUH framework, the total outflow, $Q_O(t)$, is represented as a convolution over all flow inputs to the sewer network:

$$\begin{split} Q_{O}(t) &= Q_{BWF,O}(t) + Q_{GWI,O}(t) + Q_{RDII_{fast},O}(t) + Q_{RDII_{slow},O}(t) \\ &= \sum_{k} \int_{0}^{t} Q_{I,k}(\tau) \, g_{O,k}(t-\tau) \, \mathrm{d}\tau \end{split} \tag{1}$$

Here, $k = \{\text{BWF}, \text{GWI}, \text{RDII}_{fast}, \text{RDII}_{slow}\}$ corresponds to the type of flow, $Q_{I,k}(t)$ [L³T⁻¹] is the time-varying input across all sources for the kth type of flow, and $g_{O,k}(t)$ [T⁻¹] is a transfer function that accounts for the time the kth type of flow spends transiting from its point of origin in the sewer network to the outlet. The same framework can be used to estimate BWF, GWI, and RDII at any node in the sewer network (i.e., not just at the outlet node) by adjusting the input and transfer functions, $Q_{I,k}(t)$ and $g_{O,k}(t)$, so that they include only flow entering the network upstream of the node of interest; i.e., the set of all upstream nodes, $n \in S_O$, draining to the outlet node of interest, O.

The transfer function, in turn, depends on the network's width function, $W_{O,k}(x)$, $[L^{-1}]$, which is a time-invariant probability distribution of travel distances through the network, from all sources of the kth type of flow in the network to the outlet node O. The transfer function follows by convolving the width function with a transit time model of

flow through the network. Two such models are considered here (Rigon et al., 2016): (1) a kinematic wave model; and (2) a hydrodynamic dispersion model. The corresponding transfer functions are as follows:

Kinematic Wave Model:
$$g_{O,k}(t) = u_k W_{O,k}(u_k t)$$
, (2)

Hydrodynamic Dispersion Model: $g_{O,k}(t)$

$$= \int_{0}^{L_{O,k,max}} \frac{xW_{O,k}(x)}{\sqrt{4\pi D_{t}t^{3}}} \exp\left[-\frac{(x-u_{k}t)^{2}}{4D_{k}t}\right] dx, \tag{3}$$

New variables include the celerity of a flood wave u_k [L T⁻¹], the coefficient of hydrodynamic dispersion D_k [L²T⁻¹], and the longest flow path through the network to the outlet, $L_{O,k,max}$ [L].

Implementation of these equations requires the specification of a width function specific to the network of interest. Mathematically, the width function is a probability density function (PDF), defined such that the quantity $W_{O,k}(x)dx$ represents the fraction of all sources (for the kth flow type) upstream of the outlet node that are located a flow path distance x to x+dx from the outlet. As noted above, each node may have many individual sources (e.g., many residential connections draining to a single leaf node). Thus, for a finite bin width, Δx , the width function for the kth flow type can be approximated as a histogram with N_b total bins, where the magnitude of the pth bin is given as follows:

$$W_{O,k}(x_p)$$

$$= \frac{1}{\Delta x} \sum_{n \in S_O \cap x_n \in \{(p-1)\Delta x, p\Delta x\}} \frac{\text{number of type } k \text{ sources associated with the } n\text{th node}}{\text{total number of type } k \text{ sources upstream of the outlet}}$$

(4)

The sum is taken over all nodes n that are upstream of the outlet $(n \in S_O)$ and located a path length between $x_n = (p-1)\Delta x$ and $x_n = p\Delta x$ from the outlet. The total number of bins in the histogram is related to the maximum path length through the network to the outlet as follows, $N_b = \operatorname{Floor}[L_{O,k,max}/\Delta x]$, where $\operatorname{Floor}[a]$ is an operator that computes the smallest integer that is greater than or equal to a. Next, we outline the procedure to estimate varying inputs, $Q_{I,k}(t)$, and the width functions, $W_{O,k}(x_p)$ for BWF, GWI, and RDII.

2.2. Sewage inflow to the network

2.2.1. Base wastewater flow (BWF)

Given the nested nature of the main sewer lines and local drain lines, it is reasonable to assume that most of the local sewer connections discharge BWF to the outermost network nodes, referred to here as leaf nodes (Fig. 1). With this assumption, the total input of BWF, $Q_{I,BWF}$, to the network upstream of the outlet node, O, can be calculated as follows:

$$Q_{I,BWF}(t) = N_O J_{BWF}(t) \tag{5}$$

where $J_{BWF}(t)$ is the per person wastewater input flow $[L^3T^{-1}person^{-1}]$ and N_O is the total number of people contributing sewage to the network upstream of the outlet node. The time-varying per capita wastewater input function, $J_{BWF}(t)$, can be inferred from 3 conventional strategies depending on data availability: (1) direct measurements of household wastewater production, which is usually unavailable for large systems; (2) per capita water consumption (e.g., Grant et al. (2020)) assuming that a fixed fraction (e.g., 0.9) becomes wastewater, which is the most common approach used by practitioners (Capt et al., 2021; Butler et al., 2018; Jacobs and Haarhoff, 2004); and (3) wastewater production functions reported for similar sewersheds, although this approach can introduce bias due to regional variations in water use habits and climate (Dieter et al., 2018). We proposed a different approach by taking advantage of sewer observations at the sewershed outlet and by splitting the sewage input into the product of a dimensionless periodic function, called the "demand factor", that characterizes the diurnal and weekly variation of the base wastewater flow, DF(t), and the average per capita daily BWF discharged from the network at node O, \bar{q}_{RWF} [L³T⁻¹person⁻¹]. The J_{BWF} and DF(t) is then calculated as:

$$J_{BWF}(t) = DF(t) \bar{q}_{BWF}$$
 (6a)

$$DF(t) = \frac{Q_{O,\text{dry}}(t - t_{O,h}) - Q_{O,\text{dry},\text{min}} + A_1(Q_{O,\text{dry},\text{ ave}} - Q_{O,\text{dry},\text{min}})}{(Q_{O,\text{dry},\text{ ave}} - Q_{O,\text{dry},\text{min}})(1 - A_1)}$$
 (6a)

New variables here include the dry weather sewage outflow from the network at node O, $Q_{O,\mathrm{dry}}(t-t_{O,h})$ [L³T⁻¹] where the time shift, $t_{O,h}$ [T], represents an average hydraulic residence time for water in the sewer network upstream of node O. We approximate the time shift as, $t_{O,h} = t_{O,peak} - t_{DF,peak}$, where $t_{O,peak}$ and $t_{DF,peak}$ [both T] are the time of day when the measured outflow and the demand factor peak, respectively. The flows $Q_{O,dry, min}$ and $Q_{O,dry, ave}$ [both L³T⁻¹] are the minimum and average dry weather flow measured at the outlet, respectively. The parameter A_1 is a calibration constant to ensure that DF(t) has a mean daily value equal to 1 and a minimum value equal to DF_{min} . The supplemental material presents a step-by-step description of the estimation of this diurnal function.

2.2.2. Groundwater infiltration (GWI)

While BWF enters the network at leaf nodes, GWI can enter the network through any or all nodes upstream of the outlet. The magnitude of $Q_{I,GWI}$ depends on both infrastructure health (e.g., the extent of cracks and open joints that allow for the exchange of sewage with the surrounding sediment) and the state of the shallow groundwater (e.g., the hydraulic head gradient between the sewer conduit and the surrounding aquifer, which is determined by the local hydrogeology and climate). In the absence of geographically distributed (i.e., conduitby-conduit) information on these two factors, here we assumed that the GWI attributed to each conduit is proportional to either (i) the drainage area that contributes to each sewer conduit; or (ii) the conduit length:

$$Q_{I,GWI} = \begin{cases} A_O J_{GWI,A} & \text{if contributing area is used as a proxy for GWI} \\ L_O J_{GWI,L} & \text{if conduit length is used as a proxy for GWI} \end{cases}$$

(7)

where A_O [L²] and L_O [L] are the total drainage area and total conduit length that drains to the outlet node O, respectively, and $J_{GWI,A}$ [LT⁻¹] and J_{GWLL} [L²T⁻¹] are the input groundwater flux per unit draining area and per unit length of conduit, respectively. The input fluxes J_{GWLA} and J_{GWLL} are assumed to be fixed constants and inferred using the parameter estimation approach described in Section 2.4.1.

2.2.3. Rainfall-derived infiltration and inflow (RDII)

RDII depends on rainfall characteristics (e.g., spatial distribution, duration, and intensity), sewer network structural integrity (e.g., conduit cracks and illicit connections), surface imperviousness, and the local terrain Beheshti et al. (2015). In our model, these features are embedded in the function, $J_{RDII_{fast}}$ and $J_{RDII_{slow}}$ [LT⁻¹], which represents the input of RDII_{fast} and RDII_{slow} to the sewer network per unit drainage area, respectively. The total $RDII_{fast}$ and $RDII_{slow}$ inputs are then equal to their respective J_{RDII} and the sewer network's contributing area, A_O :

$$Q_{I,\text{RDII}_{fast}}(t) = A_O J_{\text{RDII}_{fast}}(t)$$
 (8a)

$$Q_{I,\text{RDII}_{slow}}(t) = A_O J_{\text{RDII}_{slow}}(t)$$
(8b)

$$J_{\text{RDII}_{fast}}(t) = R_{fast,i} P(t)$$
 (8c)

$$J_{\text{RDII}_{slow}}(t) = R_{slow,i} P(t)$$
 (8d)

The RDII per unit area, in turn, is written as the product of the fraction of precipitation that becomes RDII for the fast response, $R_{fast,i}$

[-], and the time-varying average precipitation over the contributing area of the sewer network, P(t) [LT⁻¹] for the ith rainfall event. A similar result is obtained for the RDII slow response.

2.3. Width functions

2.3.1. Base wastewater flow

The pth bin of the width function for BWF can be written as follows (compare with (4)):

$$W_{O,\text{BWF}}(x_p) = \frac{1}{\Delta x} \sum_{n_l \in S_O \cap x_{n_l} \in [(p-1)\Delta x, p\Delta x)} \frac{N_{n_l, p}}{N_O}$$
(9)

Here, $N_{n_1,p}$ is the total number of people contributing sewage to leaf nodes upstream of the outlet $(n_l \in S_Q)$ and located at a flow path distance $x_{n_i} \in [(p-1)\Delta x, p\Delta x)$ from the outlet. The number of residential and non-residential connections to a given leaf node (i.e., $N_{n_l,p}$) can be estimated at the parcel scale from U.S. census data (Fig. 2A). In the United States, coarser-grained information on current and future population and commercial activity is frequently prepared by city and county planning departments and then aggregated into so-called Transportation Analysis Zones (TAZ, Clifton et al. (2008)). The TAZ data can be used to estimate $N_{n_l,p}$, both now and into the future, by uniformly assigning users to each leaf node within a particular TAZ polygon (Fig. 2B).

2.3.2. Groundwater infiltration (GWI)

Because GWI can enter the network at any node, the pth bin of the GWI width function is summed over all nodes (i.e., not just the leaf nodes, as in the width function for BWF above) upstream of the outlet (compare with Eqs. (4) and (9)):

$$\begin{split} W_{O,\mathrm{GWI}}(x_p) &= \frac{1}{\Delta x} \sum_{n \in S_O \, \cap \, x_n \, \in \, \lfloor (p-1) \Delta x, p \Delta x)} \\ &\times \begin{cases} \frac{A_n}{A_O} & \text{if contributing area is used as a proxy for GWI} \\ \frac{L_n}{L_O} & \text{if conduit length is used as a proxy for GWI} \end{cases} \end{split}$$

where L_n is the conduit length for link n (Fig. 2C) and A_n is the area draining to the link n (Fig. 2D). Our notation assumes that the index of the link corresponds to the index of its upstream node.

2.3.3. Rainfall derived inflow and infiltration (RDII)

For RDII fast and RDII slow, we adopt a width function that is identical to the one adopted for GWI when contributing area is used as a proxy for input to the sewer network:

$$W_{O,\text{RDII}_{fast}}(x_p) = \frac{1}{\Delta x} \sum_{n \in S_O \cap x_n \in \{(p-1)\Delta x, p\Delta x\}} \frac{A_n}{A_O}$$
(11)

The same equation is adopted for $W_{O,\mathrm{RDII}_{slow}}$. In some cases, it may be necessary to adopt more sophisticated width functions for RDII, depending on local conditions. For example, Seo et al. (2013) used two different width functions to model runoff generated by rainfall events in impervious and pervious surfaces of storm sewer systems.

2.4. Model implementation

The SS-WFIUH formulation provides a way to hydrological interpret each flow component throughout the convolution between transfer functions and input functions that are easily modulated by a few hydrodynamic (e.g., u and D) and flow parameters (e.g. \bar{q}_{BWF} , R_{fast} and R_{slow}). To illustrate this, Fig. 3 shows an example of transfer functions (excluding the RDII for slow response), input functions, and the resulting flow components GWI, BWF, and RDII at the outlet of a sewer network. Below we describe the process we used to infer unknown

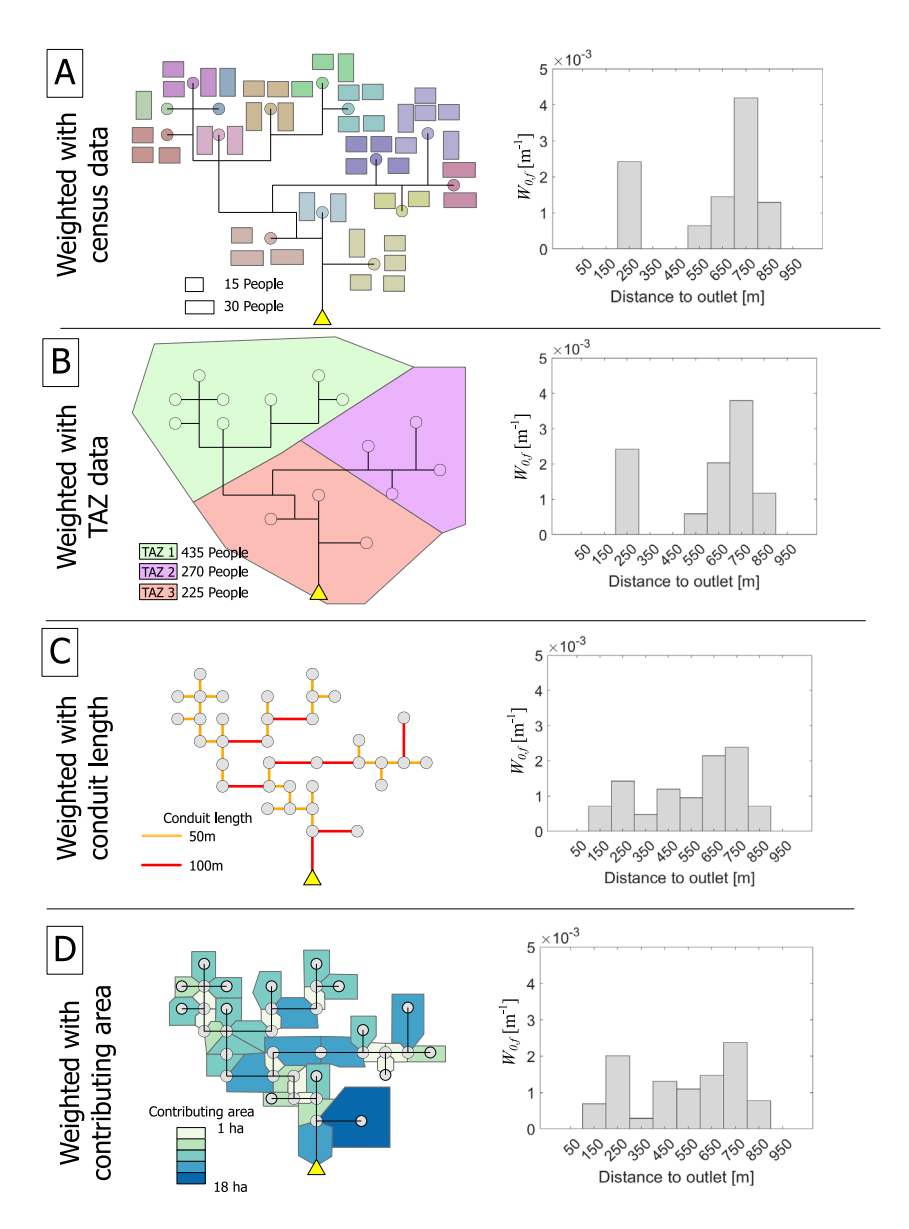


Fig. 2. Sketch of a sewershed layout highlighting the spatial distribution of the variables used to weight node contributions and the resulting weighted width function for (A) households from census data, (B) Transportation Analysis Zones (TAZ), (C) conduit length, and (D) contributing area to each sewer pipe and its corresponding weighted width function.

parameters from measured sewage flow, along with our methods for hydrograph separation and RDII estimation.

2.4.1. Parameter estimation

In the SS-WFIUH framework, the transfer function is calculated from the width function based on one of two models for sewage transit time through the network, the kinematic wave model or the hydrodynamic dispersion model (see Eqs. (2) and (3)). These two models require, in turn, the specification of two key physical properties of the system, namely, the celerity of a flood wave, u, and the coefficient of hydrodynamic dispersion D (Naden et al., 1999). For a circular channel, the celerity and dispersion coefficient can be estimated as (Seo and Schmidt, 2014)

$$u = \left[d_0 (1 - \cos \theta_I) - \frac{4}{3} R_I \right] \frac{3v_I d_0}{4B_I^2}; \quad D = C_1 \frac{Q_I}{2S_0 B_I}$$
 (12)

where the constant C_1 is defined as follows:

$$C_1 = 1 - \frac{F_I^2}{16} \left[\frac{d_0^2}{B_I^2} \left(1 - \cos \theta_I - \frac{4R_I}{d_0} \right) \right]^2$$
 (13)

New variables appearing here include the diameter of the circular cross-section d_0 [L], the initial flow velocity v_I [LT⁻¹], the initial water surface width B_I [L], the initial slope of the water surface θ_I [-], the initial hydraulic radius R_I [L], the conduit slope S_0 [-] and the Froude number F [-].

In the SS-WFIUH convolution framework (see (1) and discussion thereof), a single transfer function is specified for the entire sewer network, which implies that each network must be characterized by a single set of values for u and D. However, from the formulae provided for these two parameters above, it is clear that these two parameters will vary from conduit to conduit. Robinson et al. (1995) defined effective values of u and D for an entire river system based on hydraulic scaling relationships (Leopold and Maddock, 1953). Likewise, Naden

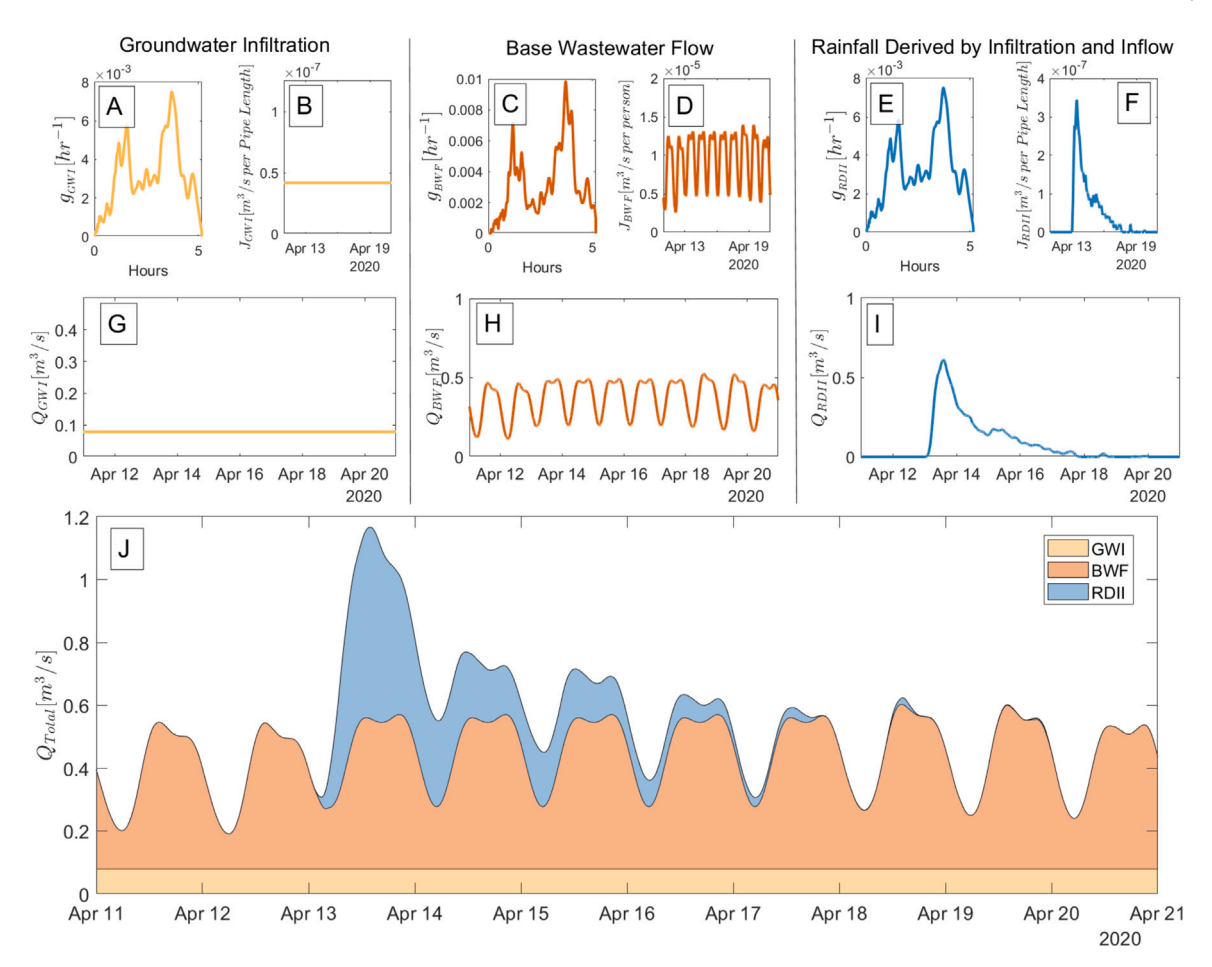


Fig. 3. Flowchart showing the schematic structure of total groundwater infiltration flow, Q_{GWI} (panel G) with transfer function g_{GWI} (panel A) and input function J_{GWI} (panel B). Total Base wastewater flow, Q_{BWF} (panel H) with transfer function g_{BWF} (panel C) and input function J_{BWF} (panel D). The total Rainfall Derived Infiltration and Inflow, Q_{RDII} (Panel I) with transfer function g_{RDII} (Panel E) and input function J_{RDII} (Panel F). This RDII component only considers fast flow response. Panel J shows the total sewage flow by adding each flow component.

et al. (1999) estimated the effective *u* and *D* for the Amazon, and the Arkansas and Red River basins, by calculating the celerity using a weighted harmonic mean of the celerity in all reaches, and the effective dispersion coefficient was calculated using a weighted arithmetic mean. In particular, the result of Naden et al. (1999) provides evidence that the equivalent celerity and dispersion coefficient may be inferred from the spatial distribution of the celerity and dispersion coefficients of individual river reaches or, in our case, for individual sewer conduits. Moreover, it is important to note that energy losses within the sewer network, particularly in manholes, can occur due to various factors, such as abrupt changes in flow at entrance points. Consequently, our equivalent parameters, *u* and *D*, implicitly incorporate these energy losses into the modeling framework.

Here, we assumed that a single set of effective parameters (u and D) apply to the transport of BWF, GWI, and RDII $_{fast}$ through the sewer network. Because the local hydrogeology also influences RDII $_{slow}$, and following previous model conceptualizations (Seo and Schmidt, 2014; Lai, 2008), this inflow was assumed to have a separate set of effective transport parameters, u_{slow} and D_{slow} .

Estimating parameters during dry weather periods: When there is no RDII, the SS-WFIUH model depends only on the BWF and GWI components. This means that the unknown parameters are u and D, along with values for the per capita daily BWF discharged at node O, \bar{q}_{BWF} , and GWI component flow, $Q_{O,\text{GWI}}$. Numerical values for these parameters were inferred by optimizing the following model-predicted

outflow from the sewer network during dry weather periods:

$$\hat{Q}_{O,\text{dry}}(t \mid \mathbf{p}) = Q_{O,\text{GWI}} + \bar{q}_{BWF} \int_{0}^{t} DF(\tau) g_{O,BWF}(t - \tau \mid \{u, D\}) d\tau$$
 (14)

where $\mathbf{p} = \{Q_{O,\mathrm{GWI}}, \bar{q}_{\mathrm{BWF}}, u, D\}$ is a vector of the model parameters. The per unit area influx of GWI to the sewer network (see Section 2.2.2) was assumed to be equal to the inferred efflux of GWI from the network: $Q_{I,\mathrm{GWI}} = Q_{O,\mathrm{GWI}}$. The parameters \mathbf{p} were inferred using Nelder–Mead simplex algorithm (Lagarias et al., 1998, as implemented in MATLAB) to minimize the sum of the square differences between sewage flow observations during dry periods, $Q_{O,\mathrm{dry}}(t)$, and SS-WFIUH predictions, $\hat{Q}_{O,\mathrm{dry}}(t|\mathbf{p})$, where the sum is taken over all flow measurements in the dry weather window of interest:

Minimize
$$Z = \sum_{j=1}^{n_{obs}} \left[\hat{Q}_{O,\text{dry}}(t_j | \mathbf{p}) - Q_{O,\text{dry}}(t_j) \right]^2$$
 (15)

Subject to $Q_{O,GWI} \ge 0$, $\bar{q}_{BWF} \ge 0$, $u \ge 0$, $D \ge 0$

Note that the per capita daily BWF, $\bar{q}_{\rm BWF}$, may be known in some localities (e.g., based on local wastewater generation studies). In such an event, the number of parameters would be reduced from 4 (in the present study) to 3.

Estimating parameters during wet weather periods: During wet weather, several additional parameters come into play, including the transport parameters u_{slow} and D_{slow} , and the rainfall fractions R_{fast}

and R_{slow} . These parameters were estimated by optimizing the following model-predicted RDII outflow from the sewer network during specific rainfall events i:

$$\hat{Q}_{O,\text{RDII}_{i}}(t | \mathbf{q}) = A_{O} R_{fast,i} \int_{0}^{t} P(\tau) g_{O,RDII_{fast}}(t - \tau | \{u, D\}) d\tau + A_{O} R_{slow,i} \int_{0}^{t} P(\tau) g_{O,RDII_{slow,i}}(t - \tau | \{u_{slow,i}, D_{slow,i}\}) d\tau$$

$$(16)$$

where $\mathbf{q}_i = \{u_{slow,i}, D_{slow,i}, R_{fast,i}, R_{slow,i}\}$ is a vector of the model parameters.

We inferred these parameters with the same Nelder–Mead simplex algorithm used for dry weather periods, but now by minimizing the sum of the square difference between observed and predicted RDII observations such as:

Minimize
$$Z = \sum_{j=1}^{n_{obs_j}} \left[\hat{Q}_{O,\text{RDII}}(t_j | \mathbf{q}_i) - Q_{O,\text{RDII}}^*(t_j) \right]^2$$
(17)

Subject to $u_{slow} > 0$, $D_{slow} > 0$, $R_{fast} \ge 0$, $R_{slow} \ge 0$

The observed RDII, $Q_{O, \mathrm{RDII}}^*(t)$, is obtained using the hydrograph separation procedure presented in the following section, and n_{obs_i} is the number of flow observations during the ith rain event. For calibration, the parameters \mathbf{q}_i are obtained for a set of events where the observed RDII is available. However, when predicting, and the RDII is not observable, the parameters \mathbf{q}_i are commonly inferred from a regression analysis between the parameters \mathbf{q}_i during the calibration period and rainfall properties. Then, when observed RDII is not available, the model parameters \mathbf{q}_i , are estimated through a non-linear equation that is fitted from rainfall volume, and the resulting vector parameters \mathbf{q}_i obtained for the calibration dataset.

2.4.2. Hydrograph separation

The flow components $Q_{O.\mathrm{GWI}}$ and $Q_{O.\mathrm{BWF}}$ estimated by the SS-WFIUH model can be used to conduct hydrograph separation of the sewage flow observations at the outlet of the sewer system, Q_{obs} . This involves extracting the flow components of Q_{obs} one-by-one, using the following expressions in sequential order:

$$Q_{O,GWI}^*(t) = Q_{O,GWI} \tag{18}$$

$$\begin{split} Q_{O,BWF}^{*}(t) &= \begin{cases} Q_{O,BWF}(t) + \Delta Q_{O,BWF} & \text{if } (Q_{O,BWF}(t) + \Delta Q_{O,BWF} + Q_{O,GWI}(t)) \\ & -Q_{obs}(t) < 0 \\ Q^{obs}(t) - Q_{O,GWI}(t) & \text{if } (Q_{O,BWF}(t) + \Delta Q_{O,BWF} + Q_{O,GWI}(t)) \\ & -Q_{obs}(t) \geq 0 \end{cases} \end{split}$$

$$\begin{aligned} &Q_{O,RDII}^*(t) \\ &= \begin{cases} Q_{obs}(t) - Q_{O,BWF}^*(t) \\ -Q_{O,GWI}(t) & \text{if } (Q_{O,BWF}^*(t) + Q_{O,GWI}(t)) - Q_{obs}(t) < 0 \\ 0 & \text{if } (Q_{O,BWF}^*(t) + Q_{O,GWI}(t)) - Q_{obs}(t) \ge 0 \end{cases} \end{aligned} \tag{20}$$

where the symbol * denotes the estimate of the hydrograph separation component, and ΔQ_{BWF} represents the expected variation of the mean sewage flow observations for dry weather periods. In practice, we suggest estimating ΔQ_{BWF} as the difference between the 95% prediction bounds and the expected value of the sewage flow from dry weather periods. Note that since $Q_{O,GWI}$ is estimated as a parameter during the calibration process of $Q_{O,BWF}$, the application of the hydrograph separation procedure based on the SS-WFIUH only requires calibrating the flow component $Q_{O,BWF}$ and estimate ΔQ_{BWF} which can be easily derived from the sewage flow observations during dry weather periods.

3. Case study

In this section, we present a proof-of-concept application where the SS-WFIUH model is used for (i) hydrograph separation and (ii) prediction of RDII during observed rainfall events. As a testbed, we use the sanitary sewer network serving the Cub Run sewershed in Fairfax County in Virginia, US (Fig. 4A). This sewershed services residents in Centreville and Chantilly, two census-designated regions in Fairfax County, Virginia (U.S.A.) (red sewer conduits in Fig. 4B). Wastewater from this sewage network discharges to the Upper Occoquan Service Authority (UOSA) water reclamation facility, which, in turn, discharges to the Occoquan Reservoir, a raw water supply for up to 1 million people in Northern Virginia. Rising sodium ion concentrations in the Occoquan Reservoir has prompted interest in developing bottom-up (stakeholder-driven) approaches for controlling sodium ion inputs to the Occoquan Reservoir, including from UOSA's reclaimed water (Bhide et al. (2021), Grant et al. (2022)). The SS-WFIUH model was developed to assist with that effort, as will be described in future publications.

The model was calibrated to hourly sewage flow observations at the outlet of the Cub Run sewershed over a 16-year period from January 2004 to December 2020. The sewer network has over 10,000 sewer conduits, with a total sewer conduit length of 574 km, an average slope of 2% (standard deviation of 2.5%), and an average sewer conduit diameter of 0.23 m (standard deviation of 0.11 m). Demographic information on water users within the sewershed was obtained from U.S. Census data and the Metropolitan Washington Council of Government TAZ attributes (Fig. 4C, D). According to the TAZ dataset, as of 2020, the Cub Run sewershed served 119,905 people from households and 109,617 employees from businesses.

Parcel scale data on drinking water consumption and wastewater generation were unavailable for this sewershed. Typically, we expect these user categories to have different water use cycles (Chin et al., 2000), especially given the diversity of activities encapsulated in the employee category, ranging from coffee shops to retail stores. However, for simplicity and to illustrate the potential of the SS-WFIUH, we assumed a common daily wastewater cycle for employees and residential users. Following recommendations from the local water utility company, the average daily sewage contribution per employee was assumed as 30% of the average daily sewage contribution per residential user (personal communication).

In the absence of measured BWF input fluxes, we used the backcalculation procedure described in Section 2.2.1 to infer the diurnal sewage flow cycle per residential user. To this end, we estimate the minimum demand factor, DF_{min} , and the time of the morning peak for water consumption, $t_{DF,peak}$, using flow observations at the Cub Run pump station. In particular, we identify the effects of the COVID-19 pandemic on the records and subdivide the data accordingly. Recent observations highlight the notable changes in diurnal water consumption cycles due to stay-at-home orders caused by the COVID-19 pandemic (Juela Quintuña, 2020; Abu-Bakar et al., 2021). In particular, the Fairfax county water utility company identified a lag in morning routines caused by the stay-at-home order imposed by Virginia on March 2020, where the morning peak of water consumption shifted from around 6:30 am on pre-COVID weekdays to about 8:00 am on COVID weekdays (personal communication). As a result, two different wastewater cycles must be established to represent water use habits during pre-COVID and COVID conditions. In the present analysis, we separated the Cub Run observations into a pre-COVID dataset (January 2004-February 2020) and a COVID dataset (March 2020-December 2020).

Regarding the system's minimum demand factor, the literature reports that DF_{min} ranges from 0.2 to 0.6 (Balacco et al., 2018; Cole and Stewart, 2013; Lopez Farias et al., 2018; Liu et al., 2010; Anele et al., 2018) with an expected value of 0.3 (Chin et al., 2000). Here, we used the expected $DF_{min} = 0.3$ to represent the diurnal wastewater cycle for

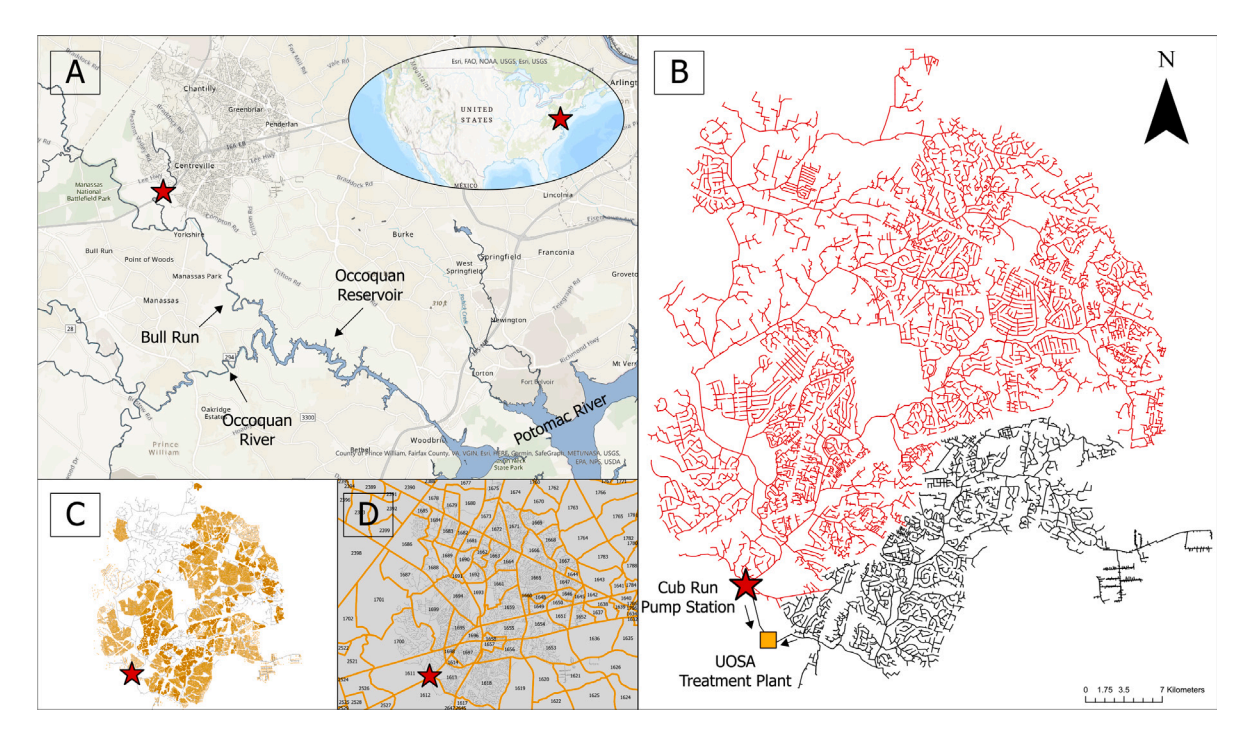


Fig. 4. (A) The Cub Run sewer network is located in Fairfax County, Virginia, U.S.A. (B) The sewershed is comprised of \approx 10,000 sewer conduits (red lines), and its outlet (red star) drains to the UOSA wastewater treatment plant. Other sewage networks that drain to the UOSA water reclamation facility (including the adjacent network indicated here by black lines) were excluded from this analysis. (C) Location of the census data within the sewershed (orange points). (D) Location of the Transportation Analysis Zones (TAZ) within the sewershed (polygons). (For interpretation of the references to color in this figure legend, the reader is referred to the web version of this article.)

pre-COVID periods. However, for COVID periods, the residential water increased and modified the diurnal pattern, including the minimum demand factor. Based on the observations at the outlet of the Cub Run sewershed and using reference values from different studies (Abu-Bakar et al., 2021; Lüdtke et al., 2021), we prescribed $DF_{min} = 0.4$ for COVID conditions.

In our analysis, we define a dry period as a period with less than 3 mm of accumulated rainfall during four consecutive days. Rainfall radar data from the Stage-IV dataset (Du, 2011) was used to define dry and wet weather periods within the system. This dataset is available from January 2004 to December 2020 with a temporal resolution of one hour and spatial resolution of roughly 4km by 4km. We assess the performance of the SS-WFIUH by conducting two analyses. First, we used the EPA's SWMM model as a reference model to compare the SS-WFIUH flow predictions during dry weather periods at the sewershed outlet and internal locations within the sewershed. The SWMM model is a higher fidelity model that incorporates the solution of the one-dimensional Saint Venant flow equation, resulting in a nonlinear parameterization with significantly higher computational cost. In this case, we injected BWF and GWI flow at each node element in the SWMM model. The BWF was estimated using the census data, and the daily average sewage flow per residential user was calculated from the back-calculation procedure presented for J_{BWF} . The GWI injected at each node was proportional to the downstream conduit length, and the sum of all the GWI input was equal to the GWI estimated from the SS-WFIUH model.

Second, we assessed the performance of the SS-WFIUH in predicting RDII at the Cub Run pump station for wet weather periods. To this end, We used the RTK unit hydrograph method as our reference model. This method is widely used by practitioners and is implemented in the SWMM model under the SSOAP toolbox (Vallabhaneni et al., 2012). In the *RTK* method, the RDII is decoupled and later aggregated into three triangular unit hydrographs related to a fast, medium, and slow

response. Each triangular unit hydrograph is determined by three parameters R, T, and K, for a total of nine parameters, wherein R denotes the fraction of rainfall falling on the sewershed that enters sewer pipes as RDII, T is the time to the peak value of RDII in hours, and K is the ratio of recession time of RDII to T (Vallabhaneni et al., 2008). We used 100 wet weather events from 2004 to 2016 for calibration and 30 wet weather events from 2017 to 2020 for validation. For the validation, we estimated the model parameters for both the RTK and SS-WFIUH models using a regional regression model using the parameters obtained during the calibration process and the total accumulated precipitation during the wet weather period.

4. Results and discussion

4.1. Estimation of the wastewater diurnal cycle

During dry weather periods, sewage flow observations at the Cub Run sewershed outlet are characterized by an average daily flow during weekdays and weekends of approximately $0.4\,\mathrm{m}^3\mathrm{s}^{-1}$ (standard deviation of approximately 0.12 m³s⁻¹) for the pre-COVID period and $0.41 \,\mathrm{m}^3 \mathrm{s}^{-1}$ (standard deviation of $0.12 \,\mathrm{m}^3 \mathrm{s}^{-1}$) for the COVID period. Overall, during the stay-at-home mandate, the wastewater contribution from commercial and business activities is expected to decrease; however, the differences between pre-COVID and COVID periods are relatively minor. This persistence in flow patterns can be explained by an increase in wastewater production from residential users that compensates for the reduction from industrial users. Similar behavior has been observed in other sewershed systems (Li et al., 2021). We observed that although the average daily sewage only increased by 2.5%, the minimum sewage flow increased by 10% during COVID conditions, going from $0.18\,\mathrm{m}^3\mathrm{s}^{-1}$ for pre-COVID to $0.20\,\mathrm{m}^3\mathrm{s}^{-1}$ for COVID periods.

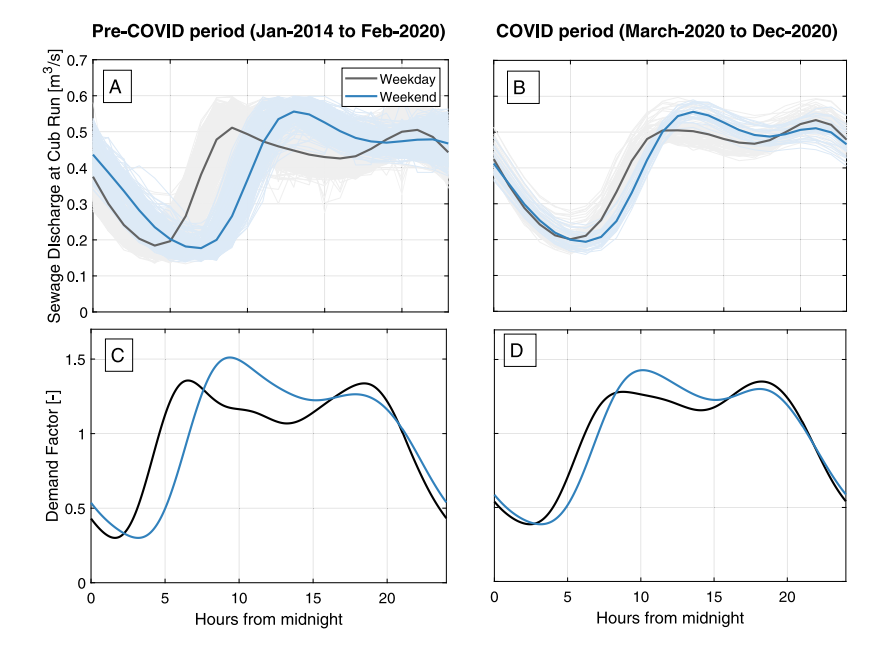


Fig. 5. Average diurnal wastewater flow from observations in dry weather periods at the Cub Run pump station. Two distinctive diurnal patterns are detected: (A) Before and (B) After the first COVID-19 lockdown that was put in place in March 2020. Panels (C) and (D) show the respective Diurnal Factors estimated by re-scaling and shifting the observed average diurnal cycles using the procedure presented in Section 2.2.1.

A Fourier spectral decomposition of the sewage flow observations at the Cub Run outlet shows that there are distinctive diurnal cycles for weekdays and weekends and also for pre-COVID and COVID conditions (Fig. 5A,B). First, let us focus on the two daily peaks of sewage flow. For pre-COVID periods (Fig. 5A), the peaks occur at 9 am and 9 pm on weekdays and at 2 pm and 10 pm on weekends. On the other hand, for COVID conditions (Fig. 5B), the diel cycle changes, resulting in a later morning peak for weekdays (it shifts to 11 am) and an earlier night peak for the weekends (it shifts to 9 pm). The timing for the other peaks remains the same. These differences between the pre-COVID and COVID sewage patterns can be explained by a delayed routine, where typical practices of personal and domestic hygiene changed during stayat-home orders. Based on the back-calculation procedure presented in Section 2.2.1, our estimate of the average hydraulic response time for the sewershed is $\bar{t}_h = 3 \, \text{h}$. This time scale is estimated as the difference between the first peak of the sewage observations (11:00 am) and the first peak of water consumption (8:00 am) on weekdays during COVID conditions. Similar results are obtained by using weekends or pre-COVID conditions. With this information, we calculate the typical diurnal variation of the demand factor for pre-COVID (Fig. 5C) and COVID (Fig. 5D) periods.

4.2. Estimation of model parameters and transfer functions

We estimated SS-WFIUH parameters for dry weather periods for both pre-COVID and COVID periods using the procedure presented in Section 2.4 and by using as "observation" the diurnal cycle obtained from the Fourier spectral decomposition of the sewage flow observations at the Cub Run. For pre-COVID periods: $u=0.93\,\mathrm{ms^{-1}}$, $D=1.2\,\mathrm{m^2s^{-1}}$, $Q_{GWI}=0.037\,\mathrm{m^3s^{-1}}$, and $\bar{q}_{BWF}=54\,\mathrm{gal}\,\mathrm{day^{-1}person^{-1}}$. For COVID periods: $u=0.92\,\mathrm{ms^{-1}}$, $D=1.5\,\mathrm{m^2s^{-1}}$, $Q_{GWI}=0.032\,\mathrm{m^3s^{-1}}$, and $\bar{q}_{BWF}=56\,\mathrm{gal}\,\mathrm{day^{-1}person^{-1}}$. Because the uncertainty of the parameter estimation approach depends on the number of unknown parameters, the use of local information to constrain \bar{q}_{BWF} can potentially improve the parameter estimates, especially the one for Q_{GWI} .

We performed a sensitivity analysis for the parameters u, D, Q_{GWI} and \bar{q}_{BWF} by repeating the calibration process for the ten driest weather periods observed in pre-COVID conditions. The selection of the events was based on the lowest observed rainfall accumulation

during two consecutive weeks. The estimated parameters for the ten dry-weather events are shown in Fig. 6. Note that the Q_{GWI} in Fig. 6A is presented as the proportion of the total sewage flow contribution. In general, the four parameters display low variability between the ten driest events and the diurnal cycle obtained from the Fourier spectral decomposition of sewage flow observations, demonstrating the calibration process's robustness and stability. From this sensitivity analysis, we can also infer that the average contribution of GWI for the ten driest weather events is around 8.2% of the total sewage flow observed at the Cub Run sewershed outlet.

Overall, all parameters are very similar between the pre-COVID and COVID periods. However, some differences are worth highlighting. First, during dry-weather periods, groundwater contributions (Q_{GWI}) are consistently significant, representing approximately 9.4% and 7.8% of the total sewage flow contribution for pre-COVID and COVID periods, respectively. When the average of the sensitivity analysis results is used (from the ten driest weather events), this percentage is about 8.2% for pre-COVID conditions. This statistic is vital to assess the structural condition of the sewer network and serves as a guide for potential interventions to minimize extraneous groundwater flows into the sanitary sewer system. Furthermore, this estimate of \mathcal{Q}_{GWI} provides a unique physics-based perspective by including hydrodynamics (u and D) and sewer network connectivity factors in the parameter estimation approach, a more robust approach than the empirical methods commonly used in the literature (Neshaei et al., 2017; Crawford et al., 1999; Mitchell et al., 2007; Hey, Gerly and Jönsson and Mattsson, 2016). For instance, it is common practice to assume that sewage flow observations during the nighttime of dry-weather periods are mostly groundwater (US Environmental Protection Agency, 2014) or to estimate it from natural tracers or pollutant load mass balances (Hey, Gerly and Jönsson and Mattsson, 2016). The latter approach can incur in significantly higher technical challenges and financial costs.

Second, we estimate that the proportion of average daily wastewater per residential user is $\bar{q}_{BWF}=54\,\mathrm{gal\,day^{-1}person^{-1}}$ during pre-COVID conditions. This flux increased by 3.2% during COVID conditions, consistent with the 2.5% increase observed for the sewage flow at Cub Run. Because we assumed that employees contribute 30% of \bar{q}_{BWF} , the average daily sewage contribution for employees is approximately $16.2\,\mathrm{gal\,day^{-1}person^{-1}}$. Putting this into the context of

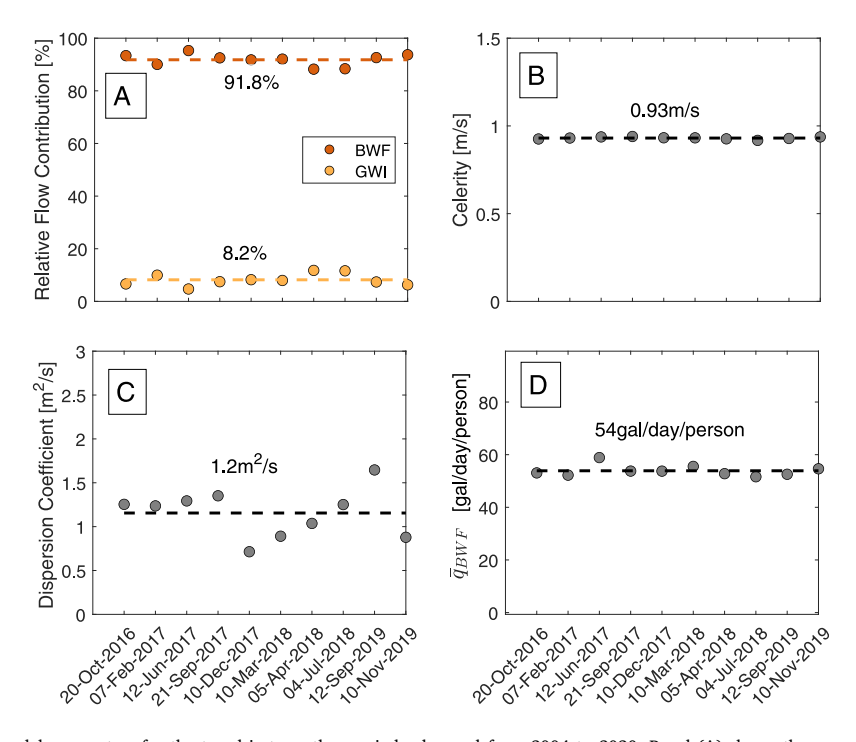


Fig. 6. Estimation of SS-WFIUH model parameters for the ten driest weather periods observed from 2004 to 2020. Panel (A) shows the proportion of GWI with respect to total sewage flow, panel (B) the celerity coefficient u, panel (C) the diffusion coefficient D, and panel (D) the average daily sewage flow per residential user \bar{q}_{BWF} .

national and local wastewater contribution statistics is important. We can calculate the effective daily sewage flow per residential user within the system by allocating the employees' contributions to the overall flow being delivered to the network. In other words, this is the flux of an equivalent system with only residential users. Given that the system services 119,908 residential users from households and 109,617 employees (who likely contribute flux during their work hours but do not live in the area), we can infer that on average person living in the Cub Run sewershed contributes (54 gal day⁻¹ person⁻¹ × $119,902 \text{ people} + 16.2 \text{ gal day}^{-1} \text{ person}^{-1} \times 109,617 \text{ people})/(119,902 \text{ people})$ = 68.8 gal day⁻¹. Assuming that the proportion of water use that becomes wastewater is 90% (return factor of 0.9) the average wastewater contribution for the US is 82 gal day-1 (Dieter et al., 2018), for Virginia is 72 gal day⁻¹ (Dieter et al., 2018), and for Fairfax county is 69 gal day⁻¹ (https://www.fairfaxva.gov/home/showdocument?id= 424, http://www.virginiaplaces.org/watersheds/WaterPlantFactSheet. pdf, accessed 14 June 2022). The SS-WFIUH estimate of 68.8 gal day⁻¹ is very similar when compared with the county estimate of 69 gal day^{-1} .

Regarding the system's transfer functions, we found that due to the high residential density in the Cub Run sewershed, the two transfer functions, g_{BWF} and g_{GWI} (or g_{RDII} for fast response), are only slightly different. The main difference is observed for the first peak, which occurs around 1 h for g_{BWF} and 1.5 h for g_{GWI} (Fig. 7). In general, however, these functions can be significantly different depending on the spatial distribution of residential users and network layout, which is dictated by the urban planning design.

4.3. Model validation for dry periods and application of hydrograph separation

We compared the SS-WFIUH output predictions for dry weather events by using the Kling–Gupta efficiency (KGE), which is a measure of the distance away from the point of the ideal model (i.e., higher-fidelity SWMM model) performance (Gupta et al., 2009). For this comparison, we used the SS-WFIUH to calculate the total sewage flow for all the nodes comprising the 10,000 sewer conduits within the Cub Run sewer

network. To this end, for the SS-WFIUH, we adjusted the input and transfer functions so that they include only flow entering the network upstream of the node of interest and by keeping the model parameters estimated using the observations at the Cub Run sewer outlet. Overall, the SS-WFIUH model reproduces the SWMM results with KGE statistics typically of 0.95 (Fig. 8) - a KGE of 1 indicates that the SS-WFIUH perfectly reproduces the SWMM outputs. We hypothesize that the lower KGEs (around 0.8) observed for some conduits (Fig. 8A,B) can be explained by noting that in our lumped model we have represented the hydraulics of the entire system with the two hydrodynamic parameters u and D. The errors resulting from this simplified conceptualization of the system will likely be most pronounced in smaller conduits with flow lower than 5 L s⁻¹. Indeed an interesting topic for future research would involve characterizing the relationship between these "equivalent parameters" in the lumped model and the actual spatial variability of local hydraulic parameters such as slope, diameter, and pipe material.

Recall that the SS-WFIUH model for dry periods only uses two effective hydrodynamic parameters (u and D) calibrated with information at the outlet of the system. These parameters result in synchronicity between the SS-WFIUH and SWMM results (Fig. 8C-F) and corroborate our estimate of a 3-hr mean hydraulic response time. If this time scale were incorrect, the model signals would have a noticeable phase lag. Furthermore, the SS-WFIUH model reproduces the response of the SWMM model for the internal conduits, increasing our confidence in the spatially distributed estimates of sewage flow components. In general, the ability of the SS-WFIUH to reproduce a significantly more complex model with a simple linear conceptualization makes it an appealing tool for systematic analyses of sewershed dynamics with a minimal computational burden. This is a major benefit when compared with models such as EPA SWMM, which are constrained by a detailed description of individual sewer conduit geometry (e.g., elevation, slope, material, and diameter), resulting in significant computational requirements.

From the spectral analysis of dry weather periods during pre-COVID conditions, the range between the expected hourly sewage observations

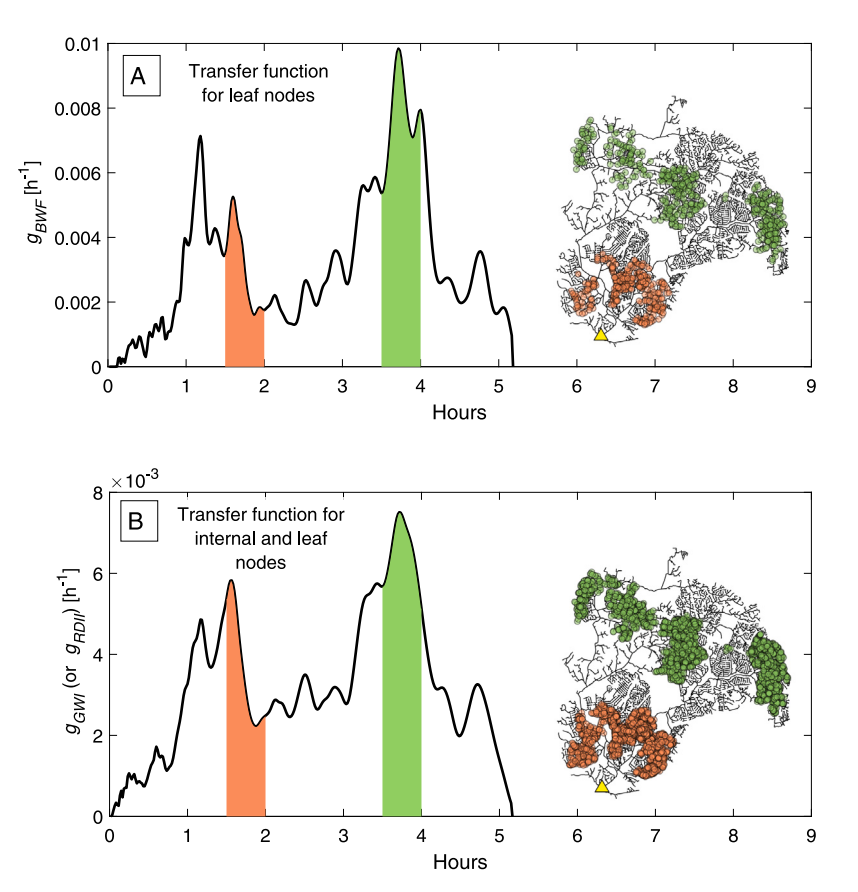


Fig. 7. (A) Transfer function, g_{BWF} , calculated with the TAZ dataset. (B) Transfer function, g_{GWI} (or g_{RDII} for fast response). The colored areas within the transfer functions highlight the sewage contribution from the locations shown in the sewer network insets. (For interpretation of the references to color in this figure legend, the reader is referred to the web version of this article.)

and the 95% confidence interval was estimated to be 0.035 m³ s⁻¹. We used this value to define the magnitude of ΔQ_{BWF} for the hydrograph separation procedure. For illustration purposes, we performed a hydrograph separation for three significant wet weather events (Fig. 9). This procedure is an efficient and simple approach to identifying both the RDII and GWI components based on a more physical representation than traditional approaches (Neshaei et al., 2017; Crawford et al., 1999; Mitchell et al., 2007; Hey, Gerly and Jönsson and Mattsson, 2016).

4.4. Model validation for RDII predictions

The calibration results of the SS-WFIUH model to predict RDII shows that this model is able to satisfactory capture the RDII signature with an average KGE of 0.66 (standard deviation of 0.2). This is significantly better than the RTK method performance, which has an average KGE of 0.49 (standard deviation of 0.34) (Fig. 10 Panel I). In particular, the SS-WFIUH model has only two events with a KGE less than 0, while the RTK method has nine events. The SS-WFIUH model outperformed the RTK method, demonstrating that it is possible to create a more accurate model of sewage flow dynamics in a system by considering the sewer network and the spatial distribution of water inputs when constructing the transfer function. This contrasts with the RTK method, which uses an ad-hoc synthetic approach with more parameters (9 parameters) than the used for the SS-WFIUH model (6 parameters), (u_{fast} , D_{fast} , u_{slow} , D_{slow} , R_{fast} , and R_{slow}).

For the validation dataset, the SS-WFIUH model still outperforms the KGE method by showing a mean KGE of 0.33 (standard deviation of 0.3) for the SS-WFIUH model, while the RTK method has a mean KGE of 0.13 (standard deviation of 0.44). Overall, the performance of the models decreased on the validation datasets. This difficulty in predicting RDII stems from various factors, including changes in

climate patterns over time, structural damage in sewage collection systems, and the presence of illegal connections between storm drains and sanitary sewers. Consequently, estimating model parameters for RDII prediction becomes a daunting task, as they are often contingent on uncertain variables and unknown quantities. Based on the regression analysis to estimate model parameters for wet weather events during the validation period, it was observed that only the parameters u_{slow} , R_{fast} , and R_{slow} showed a significant correlation with total rainfall volumes (see Figures S1-S2 and corresponding text in the SI). Notably, the parameter R_{slow} exhibited a statistically significant positive trend over the calibration period (see SI), which may indicate that the contribution of RDII inflow within the Cub Run sewershed is increasing over time. The underlying causes for this result are not clear, but could include deliberate changes in the storm and sanitary sewer infrastructure (e.g., related to the discharge of contaminated stormwater to the sanitary sewer system following storm events), rising groundwater levels in the region, and possibly infrastructure deterioration (e.g., pipe cracks), although the sanitary sewer system is quite well maintained in this region.

5. Limitations and future work

We focused on the parameterization of J_{GWI} and J_{RDII} as a function of pipe length or contributing area; however, we envision future implementations where other sewer conduit characteristics such as conduit age and material in addition to groundwater dynamics information can be used as predictors. Furthermore, it is feasible to conceptualize the hydrodynamic parameters u and D as a function of Q_{BWF} , Q_{GWI} , and Q_{RDII} . These could allow further improvements in the description of the system's residence time distribution, which is a key control in the evolution of biochemical processes and solute concentrations within

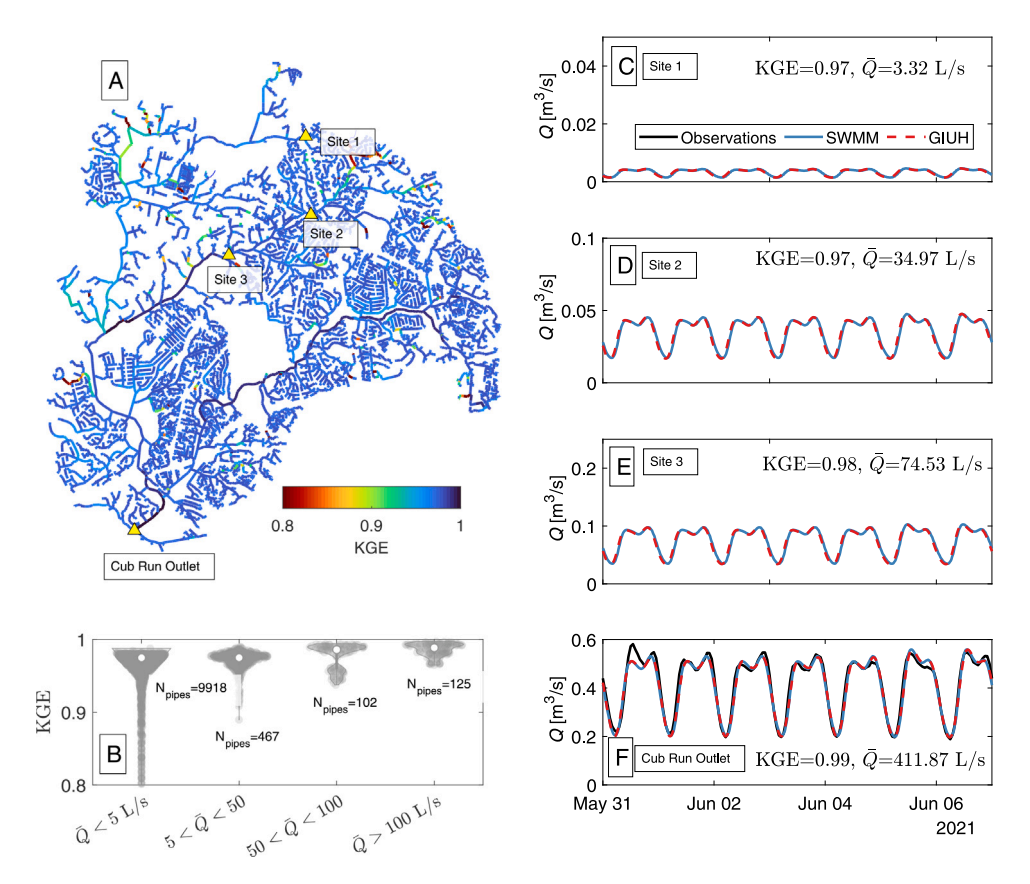


Fig. 8. Comparison of sewage flow outputs between the SS-WFIUH model and SWMM model for dry weather periods. Panel (A) shows the KGE of the estimated sewage flow series at each sewer pipe by assuming the SWMM output as the reference sewage flow and the SS-WFIUH as the estimated sewage flow. Panel B shows violin plots with the KGE aggregated into four distinctive sewage flow scales, $\bar{Q} < 5$ L/s, $5 < \bar{Q} < 50$, $50 < \bar{Q} < 100$, and $\bar{Q} > 100$ L/s. The sewage flow time series from the SS-WFIUH and SWMM at the sewershed outlet and three other locations representing the distinctive aggregation of sewage flow within the sewer network are shown in Panels C, D, E, and F. Note that Panel F also shows the observations from the Cub Run pump station.

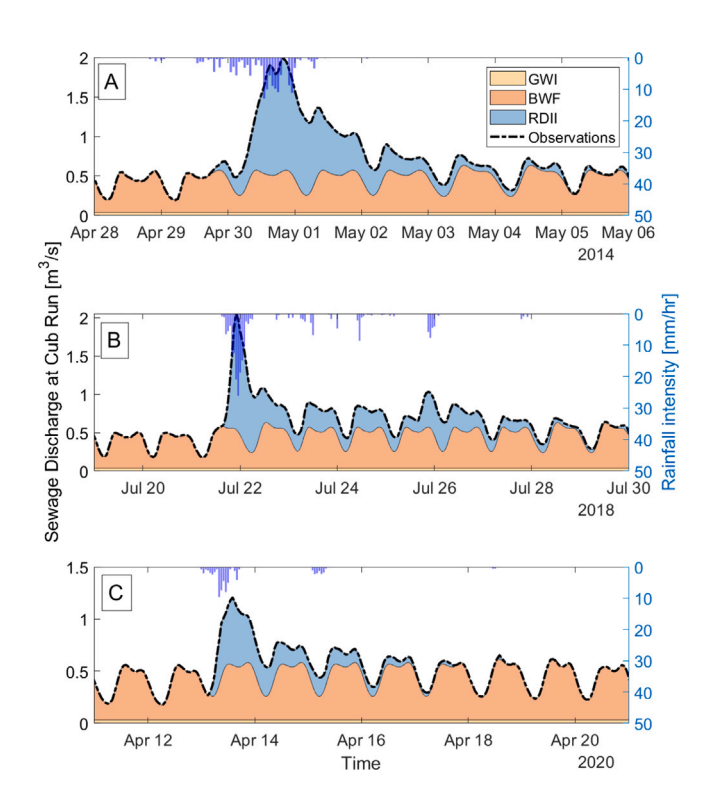


Fig. 9. Hydrograph separation at the Cub Run sewershed outlet for three events (Panel A, B, and C) by using the SS-WFIUH.

urban systems (Kaushal and Belt, 2012). Future efforts must explore the correlation between flow components and the parameters u and D.

In our testbed, we focused on hydrograph separation as a useful application of the SS-WFIUH model. To this end, we estimated u and D based on sewage flow observations; however, as pointed out by Naden et al. (1999), these parameters may be inferred from the spatial distribution of the celerity and diffusion coefficients of individual links (sewer conduits). The inference of equivalent parameters from distributed parameters is imperative to bridge the convergence from distributed models to lumped models. In particular, the use of the SS-WFIUH may provide insights in this direction by conducting future research in investigating the relation between lumped parameters in SS-WFIUH and the individual parameters at each sewer conduit extracted from distributed models such as the SWMM model.

The transfer function in the SS-WFIUH model is time-invariant, implying that the spatial distribution of water users remains constant over the domain. This is a reasonable assumption over a few years; however, significant demographic changes can occur at the scale of decades, resulting in substantial changes in the transfer functions. For instance, the transfer functions for population projections (e.g., for 2100 in the Virginia TAZ) should be adjusted to reflect the spatial patterns of water users. This adjustment can be approximated by recalculating the weighted width function based on the spatial distribution for the projected water users. This is particularly interesting for urban planning purposes in light of accelerated urban growth and gentrification. Furthermore, leveraging descriptors of the width function, (Moussa, 2008; Perez et al., 2018, 2019) could provide valuable insights into understanding changes in sewage fluxes, especially when dealing with the preliminary evaluation of different sewer system configurations. Finally, future applications on the SS-WFIUH for RDII prediction should

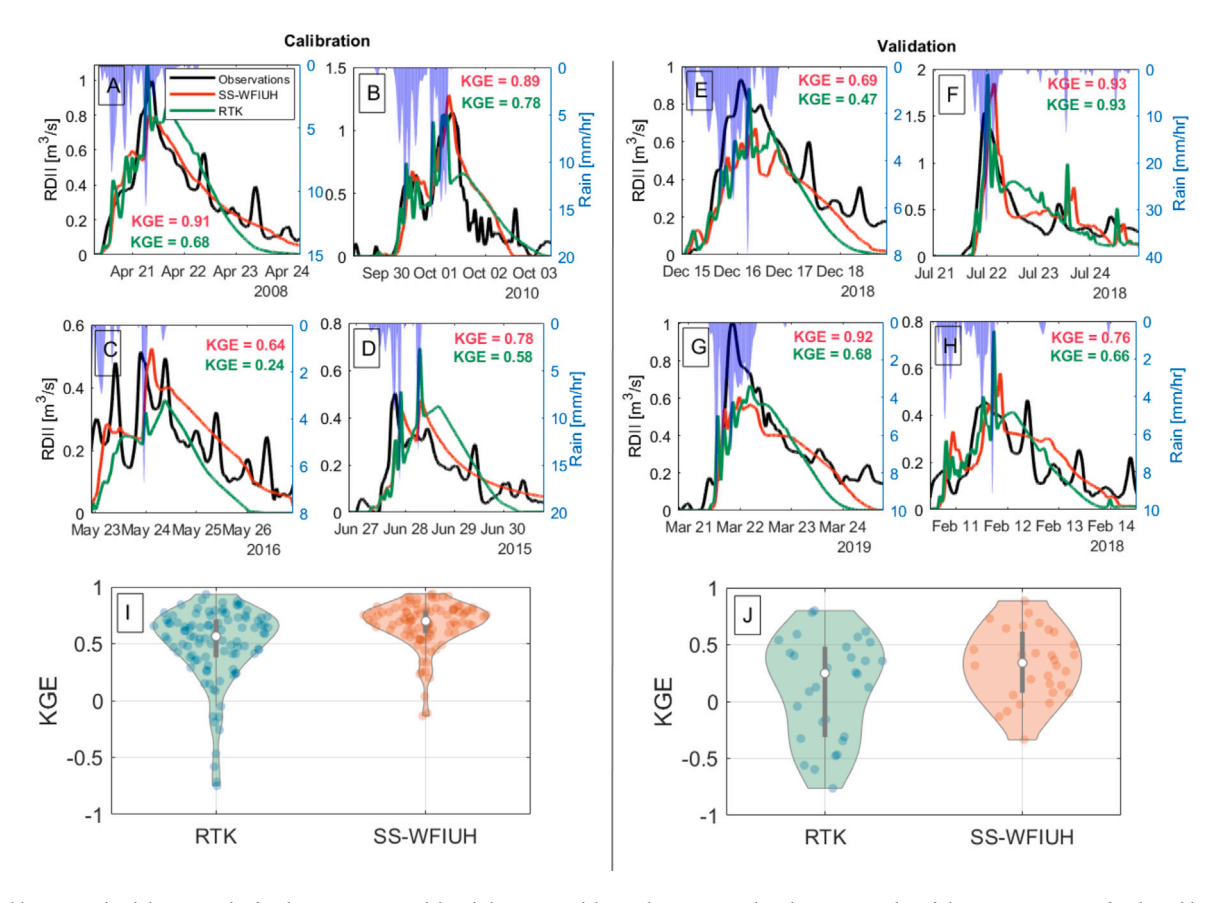


Fig. 10. Calibration and validation results for the SS-WFIUH model and the RTK model. Panels A, B, C, and D show 4 examples of the RDII estimations for the calibration dataset and Panels E, F, G, and H for the validation dataset. Panel I shows the KGE for 100 wet weather events in the calibration dataset and Panel J for 30 wet weather events for the validation dataset.

explore more explanatory variables, and not only the total rainfall volume, to better estimate model parameters.

6. Conclusions

This study presents the formulation of the Width Function Instantaneous Unit Hydrograph (WFIUH) to model Sanitary Sewer (SS) systems: the SS-WFIUH model. This is a physics-based model that incorporates the solution of the diffusion approximations to the Saint Venant Equations to conduct sewage flow routing within a lumped conceptualization of the sewershed system. The use of the SS-WFIUH model requires the definition of the input fluxes related to Groundwater Infiltration (J_{GWI}) , Base Wastewater Flow (J_{BWF}) , and Rainfall-Derived Infiltration and Inflow ($J_{RDII_{fast}}$ and $J_{RDII_{slow}}$), the sewer network topology and geometry. The SS-WFIUH for dry weather events only requires two parameters to encapsulate the hydrodynamics of sewage flow, the flow celerity u, and the dispersion coefficient D. For wet weather events, the SS-WFIUH requires four additional parameters u_{slow} , D_{slow} , R_{fast} , and R_{slow} . Using a real testbed, we showed that the SS-WFIUH reproduces the results of the EPA SWMM model for dry weather events with significantly less computation burden. For wet weather events, we showed the SS-WFIUH outperforms the RTK unit hydrograph method, widely used by practitioners. Overall, we can summarize the main characteristics and contributions of the SS-WFIUH model as follows:

 The SS-WFIUH model incorporates individual transfer functions to represent the flow components from the Groundwater Infiltration (GWI), Base Wastewater Flow (BWF), and Rainfall-Derived Infiltration and Inflow (RDII), with the latter divided into a "fast response" and "slow response".

- 2. The SS-WFIUH model uses the concept of weighted width function to capture the spatial distribution of input fluxes J_{GWI} , J_{BWF} , $J_{RDII_{fast}}$ and $J_{RDII_{slow}}$ within the sewershed system.
- The SS-WFIUH for the BWF component can be easily used to conduct hydrograph separation of sewage flow observations and provide a robust physics-based estimation of groundwater infiltration in sanitary sewer systems.

We envision this model as a generic tool to understand and predict the dynamics of sewer systems. Furthermore, it can be used as an engineering tool for the design of new networks and the assessment of new urban developments on the sewage flow dynamics. It can also serve as a learning tool to identify sampling locations to characterize different flow components (BWF, GWI, and RDII) and contributions from water users (e.g., residential and non-residential), which ultimately is critical to mitigating sanitary sewer overflows and the fate and transport of solutes and contaminants within wastewater systems.

Declaration of competing interest

The authors declare that they have no known competing financial interests or personal relationships that could have appeared to influence the work reported in this paper.

Data availability

The scripts to implement the SS-WFIUH are publicly available at https://github.com/gomezvelezlab/SanitarySewer-WFIUH.

Acknowledgments

This study was supported by the U.S. National Science Foundation (awards OIA-2312326, OIA-2020814, EAR-1830172, and OIA-2021015) and the U.S. Department of Energy, Office of Science, United States, Biological and Environmental Research, United States. This work is a product of two programs: (i) Environmental System Science Program, as part of the Watershed Dynamics and Evolution (WaDE) Science Focus Area at Oak Ridge National Laboratory and the IDEAS-Watersheds project, and (ii) Data Management Program, as part of the ExaSheds project.

Census data was obtained from Fairfax County's Open Geospatial Data site (https://data-fairfaxcountygis.opendata.arcgis.com/), and the TAZ data was obtained from the Metropolitan Washington Council of Governments (https://www.mwcog.org). Both datasets were accessed on June 14, 2022. The scripts to implement the SS-WFIUH are publicly available at https://github.com/gomezvelezlab/SanitarySewer-WFIUH.

Appendix A. Supplementary data

Supplementary material related to this article can be found online at https://doi.org/10.1016/j.watres.2023.120997.

References

- Abu-Bakar, H., Williams, L., Hallett, S.H., 2021. Quantifying the impact of the COVID-19 lockdown on household water consumption patterns in England. npj Clean Water 4 (1), 13.
- Anele, A., Todini, E., Hamam, Y., Abu-Mahfouz, A., 2018. Predictive uncertainty estimation in water demand forecasting using the model conditional processor. Water 10 (4), 475.
- Balacco, G., Gioia, A., Iacobellis, V., Piccinni, A., 2018. At-site assessment of a regional design criterium for water-demand peak factor evaluation. Water 11 (1), 24.
- Beheshti, M., Sægrov, S., Ugarelli, R., 2015. Infiltration / inflow assessment and detection in urban sewer system. Vann (01), 24–34.
- Bhide, S.V., Grant, S.B., Parker, E.A., Rippy, M.A., Godrej, A.N., Kaushal, S., Prelewicz, G., Saji, N., Curtis, S., Vikesland, P., Maile-Moskowitz, A., Edwards, M., Lopez, K.G., Birkland, T.A., Schenk, T., 2021. Addressing the contribution of indirect potable reuse to inland freshwater salinization. Nature Sustain. 4 (8), 699–707
- Butler, D., Digman, C., Makropoulos, C., Davies, J.W., 2018. Urban Drainage, Fourth Edition CRC Press.
- Capt, T., Mirchi, A., Kumar, S., Walker, W.S., 2021. Urban water demand: Statistical optimization approach to modeling daily demand. J. Water Resour. Plan. Manag. 147 (2), 04020105.
- Chin, D.A., Mazumdar, A., Roy, P.K., 2000. Water-Resources Engineering, Vol. 12. Prentice Hall Englewood Cliffs.
- Clifton, K., Ewing, R., Knaap, G.J., Song, Y., 2008. Quantitative analysis of urban form: A multidisciplinary review. 1, pp. 17–45. http://dx.doi.org/10.1080/17549170801903496.
- Cole, G., Stewart, R.A., 2013. Smart meter enabled disaggregation of urban peak water demand: precursor to effective urban water planning. Urban Water J. 10 (3), 174–194.
- Crawford, D., Eckley, P.L., Pier, E., 1999. Methods for estimating inflow and infiltration into sanitary sewers. J. Water Manag. Model. 6062.
- Di Lazzaro, M., Zarlenga, A., Volpi, E., 2015. Hydrological effects of within-catchment heterogeneity of drainage density. Adv. Water Resour. 76, 157–167.
- Dieter, C., Maupin, M., Caldwell, R., Harris, M., Ivahnenko, T., Lovelace, J., Barber, N., Linsey, K., 2018. Estimated use of water in the United States in 2015. U.S. Geological Survey Circular. (765).
- Du, J., 2011. GCIP/EOP surface: Precipitation NCEP/EMC 4KM gridded data (GRIB) stage IV data. Version 1.0. In: UCAR/NCAR Earth Observing Laboratory.
- Gonzalez, R., Curtis, K., Bivins, A., Bibby, K., Weir, M.H., Yetka, K., Thompson, H., Keeling, D., Mitchell, J., Gonzalez, D., 2020. COVID-19 surveillance in southeastern virginia using wastewater-based epidemiology. Water Res. 186.
- Grant, S.B., Duong, K., Pierce, G., Feldman, D., Zanetti, E., McNulty, A., 2020. From yards to cities: A simple and generalizable probabilitic framework for upscaling outdoor water conservation behavior. Environ. Res. Lett. 15.
- Grant, S.B., Rippy, M.A., Birkland, T.A., Schenk, T., Rowles, K., Misra, S., Aminpour, P., Kaushal, S., Vikesland, P., Berglund, E., Gomez-Velez, J.D., Hotchkiss, E.R., Perez, G., Zhang, H.X., Armstrong, K., Bhide, S.V., Krauss, L., Maas, C., Mendoza, K., Shipman, C., Zhang, Y., Zhong, Y., 2022. Can common pool resource theory catalyze stakeholder-driven solutions to the freshwater salinization syndrome?. Environ. Sci. Technol..

Grant, S.B., Saphores, J.D., Feldman, D.L., Hamilton, T.D., Cook, P.L., Stewardson, M., Sanders, B.F., Levin, L.A., Ambrose, R.F., Deletic, A., Brown, R., Jiang, S.C., Rosso, D., Cooper, W.J., Marusic, I., 2012. Taking the waste out of wastewater for human water security and ecosystem sustainability. Science 337, 681–686.

- Gupta, H.V., Kling, H., Yilmaz, K.K., Martinez, G.F., 2009. Decomposition of the mean squared error and NSE performance criteria: Implications for improving hydrological modelling. J. Hydrol. 377 (1), 80–91.
- Hey, Gerly and Jönsson, K., Mattsson, A., 2016. The impact of infiltration and inflow on wastewater treatment plants: A case study in Sweden. VA-Teknik Sodra, Rapport Nr.
- Jacobs, H., Haarhoff, J., 2004. Structure and data requirements of an end-use model for residential water demand and return flow. Water SA 30 (3), 293-304.
- Juela Quintuña, D.M., 2020. Estimated impact of COVID-19 on water needs and volume and quality of wastewater. SSRN Electron. J. 1 (2003), 1-6.
- Karpf, C., Krebs, P., 2011. Quantification of groundwater infiltration and surface water inflows in urban sewer networks based on a multiple model approach. Water Res. 45 (10), 3129–3136.
- Kaushal, S.S., Belt, K.T., 2012. The urban watershed continuum: evolving spatial and temporal dimensions. Urban Ecosyst. 15 (2), 409–435.
- Lagarias, J.C., Reeds, J.A., Wright, M.H., Wright, P.E., 1998. Convergence properties of the Nelder–Mead simplex method in low dimensions. SIAM J. Optim. 9 (1), 112–147, Publisher: Society for Industrial and Applied Mathematics.
- Lai, F.-h., 2008. Review of sewer design criteria and RDII prediction review of sewer design criteria and RDII prediction methods. Environ. Protect. (January), 1–30.
- Leopold, L.B., Maddock, T., 1953. The Hydraulic Geometry of Stream Channels and Some Physiographic Implications, Vol. 252. US Government Printing Office.
- Li, D., Engel, R.A., Ma, X., Porse, E., Kaplan, J.D., Margulis, S.A., Lettenmaier, D.P., 2021. Stay-at-home orders during the COVID-19 pandemic reduced urban water use. Environ. Sci. Technol. Lett. 8 (5), 431–436.
- Liu, J., Zhang, R., Wang, L., 2010. Prediction of urban short-term water consumption in Zhengzhou city. In: 2010 International Conference on Intelligent Computation Technology and Automation, Vol. 2. IEEE, pp. 922–926.
- Lopez Farias, R., Puig, V., Rodriguez Rangel, H., Flores, J., 2018. Multi-model prediction for demand forecast in water distribution networks. Energies 11 (3), 660.
- Lüdtke, D.U., Luetkemeier, R., Schneemann, M., Liehr, S., 2021. Increase in daily household water demand during the first wave of the Covid-19 pandemic in Germany. Water 13 (3), 260.
- Mitchell, P.S., Stevens, P.L., Nazaroff, A., 2007. Quantifying base infiltration in sewers:
 A comparison of methods and a simple empirical solution. Proc. Water Environ.
 Fed. 2007 (4), 219–238.
- Moussa, R., 2008. What controls the width function shape, and can it be used for channel network comparison and regionalization? Water Resour. Res. 44 (8), 1–19.
- Mutzner, R., Tarolli, P., Sofia, G., Parlange, M.B., Rinaldo, A., 2016. Field study on drainage densities and rescaled width functions in a high-altitude alpine catchment. Hydrol. Process. 30 (13), 2138–2152.
- Naden, P., Broadhurst, P., Tauveron, N., Walker, A., 1999. River routing at the continental scale: use of globally-available data and an a priori method of parameter estimation. Hydrol. Earth Syst. Sci. 3 (1), 109–123.
- Nasrin, T., Sharma, A., Muttil, N., 2017. Impact of short duration intense rainfall events on sanitary sewer network performance. Water 9 (3), 225.
- Neshaei, S., Ahmadnejad, A., Yousefi, F., Ghanbarpour, F., 2017. Estimating ground-water and rainfall infiltration into sewerage. Int. J. Sustain. Dev. Plan. 12 (01), 185–193.
- Pangle, L.A., Diem, J.E., Milligan, R., Adams, E., Murray, A., 2022. Contextualizing inflow and infiltration within the streamflow regime of urban watersheds. Water Resour. Res. 58 (1), 1–19.
- Perez, G., Gomez-Velez, J.D., Chen, X., Scheibe, T., 2023. The directional unit hydrograph model: Connecting streamflow response to storm dynamics. J. Hydrol. 627, 130422.
- Perez, G., Mantilla, R., Krajewski, W.F., 2018. The influence of spatial variability of width functions on regional peak flow regressions. Water Resour. Res. 54, 7651–7669.
- Perez, G., Mantilla, R., Krajewski, W.F., Quintero, F., 2019. Examining observed rainfall, soil moisture, and river network variabilities on peak flow scaling of rainfall-runoff events with implications on regionalization of peak flow quantiles. Water Resour. Res. 55 (12), 10707–10726.
- Piccolroaz, S., Di Lazzaro, M., Zarlenga, A., Majone, B., Bellin, A., Fiori, A., 2016. Hyperstream: A multi-scale framework for streamflow routing in large-scale hydrological model. Hydrol. Earth Syst. Sci. 20 (5), 2047–2061.
- Rigon, R., Bancheri, M., Formetta, G., de Lavenne, A., 2016. The geomorphological unit hydrograph from a historical-critical perspective. Earth Surf. Process. Landf. 41 (1), 27–37.
- Robinson, J.S., Sivapalan, M., Snell, J.D., 1995. On the relative roles of hillslope processes, channel routing, and network geomorphology in the hydrologic response of natural catchments. Water Resour. Res. 31 (12), 3089–3101.
- Selvakumar, A., Field, R., Burgess, E., Amick, R., 2004. Exfiltration in sanitary sewer systems in the US. Urban Water J. 1 (3), 227-234.
- Seo, Y., Choi, N.-J., Schmidt, A.R., 2013. Contribution of directly connected and isolated impervious areas to urban drainage network hydrographs. Hydrol. Earth Syst. Sci. 17 (9), 3473–3483.

Seo, Y., Schmidt, A.R., 2014. Application of Gibbs' model to urban drainage networks: A case study in southwestern chicago, USA. Hydrol. Process. 28 (3), 1148–1158.

- Sherman, L.K., 1932. Stream flow from rainfall by the unit graph method. Eng. News Rec. (No. 108), 501–505.
- Sojobi, A.O., Zayed, T., 2022. Impact of sewer overflow on public health: A comprehensive scientometric analysis and systematic review. Environ. Res. 203 (April 2021), 111609
- US Environmental Protection Agency, 2014. Guide for Estimating Infiltration and Inflow. Technical report.
- Vallabhaneni, S., Burgess, E.H., 2007. Computer tools for sanitary sewer system capacity analysis and computer tools for sanitary sewer system. Environ. Protect. (October), 1–104.
- Vallabhaneni, S., Chan, C., Campbell, S., 2012. SSOAP Toolbox Enhancements and Case Study. USEPA, Cincinnati, OH.

- Vallabhaneni, S., Lai, F., Chan, C., Burgess, E.H., FIELD, R.I., 2008. SSOAP A USEPA Toolbox for Sanitary Sewer Overflow Analysis and Control Planning. Honolulu, HI.
- Volpi, E., Di Lazzaro, M., Fiori, A., 2013. Analytical modeling of the hydrologic response under moving rainstorms: Storm–catchment interaction and resonance. J. Hydrol. 493, 132–139.
- Yang, K., Smith, L.C., Karlstrom, L., Cooper, M.G., Tedesco, M., van As, D., Cheng, X., Chen, Z., Li, M., 2018. A new surface meltwater routing model for use on the greenland ice sheet surface. Cryosphere 12 (12), 3791–3811.
- Zhang, M., Liu, Y., Cheng, X., Zhu, D.Z., Shi, H., Yuan, Z., 2018a. Quantifying rainfall-derived inflow and infiltration in sanitary sewer systems based on conductivity monitoring. J. Hydrol. 558, 174–183.
- Zhang, M., Liu, Y., Dong, Q., Hong, Y., Huang, X., Shi, H., Yuan, Z., 2018b. Estimating rainfall-induced inflow and infiltration in a sanitary sewer system based on water quality modelling: which parameter to use? Environ. Sci.: Water Res. Technol. 4 (3), 385–393.